Effect of sugar cane straw ash (SCSA) as solid precursor and the alkaline activator composition on alkali-activated binders based on blast furnace slag (BFS)

J. C. B. Moraes[1], M. M. Tashima[1], J. L. Akasaki[1], J. L. P. Melges[1], J. Monzó[2], M. V. Borrachero[2], L. Soriano[2], J. Payá[2*]

[1]UNESP – Grupo de Pesquisa MAC – Materiais Alternativos de Construção. Univ Estadual Paulista, Campus de Ilha Solteira, São Paulo, Brazil.

[2]ICITECH – GIQUIMA Group - Grupo de Investigación en Química de los Materiales de Construcción. Instituto de Ciencia y Tecnología del Hormigón, Universitat Politècnica de Valencia, Valencia, Spain.

*** Corresponding author: jjpaya@cst.upv.es; tel: +34 387 75 69.**

ABSTRACT

Alkali-activated materials (AAM) comprise one of the solutions to diminish the use of Portland cement in building construction and, consequently, a reduction in the environmental problems related to CO_2 emissions and energy consumption may be achieved. These kinds of binders are obtained when a mineral precursor (calcium silicate or aluminosilicate material) is mixed with an alkaline solution. In this study, the blast furnace slag (BFS) combined with a new waste from the sugar cane industry, sugar cane straw ash (SCSA), is utilised. This new residue was studied replacing partially the blast furnace slag in BFS/SCSA proportions of 100/0, 85/15, 75/25, 67/33 and 50/50. The alkaline solution concentration plays an important role in obtaining AAM with good mechanical properties. Therefore, this paper intends to assess the influence of the activating solution (composed of sodium hydroxide and sodium silicate) through different H_2O/Na_2O (called η) and SiO_2/Na_2O (called ε) molar ratios. For BFS/SCSA proportions of 100/0 and 75/25, the η values assessed were 22, 28 and 37, whereas the ε values selected were 0 and 0.75. In order to study the effects of SCSA in the mixture, other BFS/SCSA proportions (0-50% replacement) were assessed by only η and ε ratios of 28 and 0-0.75, respectively. To reach these objectives, mortars and pastes were manufactured in order to study their behaviour in the following tests: compressive strength (3, 7, 28 and 90 days of curing at 25ºC), Fourier transform infrared spectroscopy (FTIR), thermogravimetric analysis (TGA), X-ray diffraction (XRD), mercury intrusion porosimetry (MIP) and field emission scanning electron microscopy (FESEM). The results showed that the alkaline solution influenced the compressive strength development, and specimens reached more than 60 MPa after

90 days of curing. In addition, the mortars with SCSA and without sodium silicate presented similar values of compressive strength to those samples with only BFS and sodium silicate, showing that the ash can replace the sodium silicate, which is the pollutant and an expensive chemical reagent, yielding a sustainable binder. Therefore, SCSA presented good results and is a promising material in alkali-activated binders.

KEYWORDS: environmentally friendly material, biomass waste, compressive strength, microstructural studies, sustainability

1. INTRODUCTION

Alkali-activated materials (AAM) development is one of the newest trends in binder for building construction. In a previous study it can be found more details about AMM definition, their advantages and the most common raw materials [1]. Now it will be focus on important support studies for this present research.

In recent decades, assessment of the reuse of biomass ashes in inorganic binders (mainly Portland cement) has been an important focus of attention [2]. In addition, in the last few years, the use of biomass ashes as supplementary mineral admixtures in alkali-activated BFS-based binders has notably increased [3]. The combination of BFS and palm oil fuel ashes (POFA) is noticeable [4,5]. In these studies, the authors obtained a higher compressive strength with the 20% replacement of BFS by POFA compared to the control after 28 days of curing [4]; this percentage was increased to 30% without any important loss of mixture properties [5]. In the case of residues derived from the sugarcane industry, some examples have recently been reported regarding sugarcane bagasse ash (SCBA) [6,7]. The presence of SCBA from an autocombustion process in BFS/SCBA ratio of 75/25 resulted in slightly higher compressive strength than the control after 90 days of curing. In durability studies, the alkali-activated binders were compared to Portland cement mixtures in ammonium chloride, acetic acid and sodium sulphate attacks, where the new type of binders exhibited better behaviour than conventional ones [6]. In another study with the SCBA produced in an industrial combustion, the ash can be utilised until a 40% replacement of BFS is reached, and yields an important contribution in the mechanical strength of BFS/SCBA mixtures.

Another interesting biomass derived from the sugarcane crop is sugarcane straw, which is produced in large amounts and is usually abandoned in land. This biomass could be transformed into reactive ash (sugarcane straw ash, SCSA) for reuse in inorganic binders [8]: interesting sustainability issues have been described in terms of saving energy and raw materials for cement and concrete. The SCSA is obtained from the combustion of sugar cane straw, a waste that increased in the last few years for two reasons: the expansion of sugar cane production in many countries and the trend to use a mechanized harvesting. Related the first reason, an example can be given: sugar cane production in Brazil expanded from 385,000 tons in 2005/2006 to 670,000 tons in 2015/2016, which represents an increase of 74% in only one decade [9]. The main reason for this increase is high demand in the production of ethanol [10]. Following the second reason, several protocols prohibited the open field burning in crop fields before collecting the sugar cane, due to safety and environmental issues. After the mechanised harvesting process, sugar cane straw is obtained, which is mostly left on the field to cover the bare soil; however, some of it can be reused without affecting this protection [11]. This straw presents an interesting calorific value, and there are some studies about selected ways to collect it in order to produce energy by a burning procedure; sugar cane bagasse is already being utilised in this way [11-13]. After the combustion of the straw, an ash rich in silica is generated: sugar cane straw ash (SCSA).

In an early published paper [1], SCSA was used to replace BFS in AAM. The results demonstrated the high reactivity of SCSA, especially for those mixtures activated with NaOH solution. In this case, the concentration of the solution was 8 $mol.kg^{-1}$. In addition, other alkali activators tested contained a mixture of NaOH and waterglass (studied solutions presented 0.5 and 0.75 SiO_2/Na_2O molar ratios), maintaining the concentration of Na^+ at a constant level. In this case, the goal was to produce the solubilisation of the silica present in the SCSA by means a high alkaline solution, and consequently the required quantities of NaOH and waterglass were high. In these conditions, compressive strength of 90-days mortars of BFS/SCSA activated mixtures were similar or higher than those found for only BFS activated system.

Regarding the alkaline activating solution, the reported papers showed that the most utilised alkali sources are sodium hydroxide and sodium silicate (waterglass) [14]. The concentration of these solutions and the SiO_2/Na_2O molar ratio are crucial parameters to reach interesting mechanical properties, since variations on the solution concentration and relative dosage with respect to the solid precursor can provide different compressive strengths

after a given curing age, as reported in some studies [15-17]. In this way, the influence of the solution concentration to a given solid precursor should be studied in order to achieve the optimum dosage.

Seriously, the use of silicates in the preparation of alkaline solutions is responsible for the most greenhouse gas emissions related to AAM; however, this chemical compound becomes very important in the mechanical strength development of the AAM. One possibility is to prepare sodium carbonate-silicate mixes, for partially reducing the silicate source [18]. Another possibility is replacing the waterglass with another siliceous source. Some authors used residues in the preparation of the alkaline solution, such as rice husk ash and glass waste, and obtained compressive strengths of mortars similar to the control ones prepared with sodium silicate [19-21]. Another alternative possibility is to reduce the quantity of alkali compounds (especially sodium silicate) by blending solid silica-rich wastes with the precursor. In this paper, binary BFS/SCSA systems have been tested, where one of the solid precursors (SCSA) is rich in reactive silica.

The research had two objectives: the first was to add value for an ash derived from a residue in the sugar cane industry, SCSA, as a way to reduce the use of sodium silicate in AAM; the second one was to study the influence of the alkaline solution concentration on the mechanical properties of these proposed AAM based on a BFS/SCSA binary system. SCSA was already studied as a solid precursor in a previous study [1]. In this former study, only one H_2O/Na_2O molar ratio was assessed, with different SiO_2/Na_2O molar ratios. Authors observed that the mechanical behaviour for mortars composed by BFS/SCSA activated with only sodium hydroxide is similar to the one observed for BFS mixed with NaOH and sodium silicate. This result means that the SCSA is a silica source similar than the sodium silicate in AAM. Regarding to the present study, the activating solution varied for both molar ratios: H_2O/Na_2O (called η) and SiO_2/Na_2O (called ε). The η values in the studied mixtures were 22, 28 and 37 (they were approximately to the corresponding solutions 5, 4 and 3 $mol.kg^{-1}$ of Na^+ respectively), whereas the ε values were 0 (only sodium hydroxide) and 0.75. With respect to the solid precursors, the following BFS/SCSA proportions (by weight) were assessed: 100/0, 85/15, 75/25, 67/33 and 50/50. Compressive strengths of mortars were assessed until 90 days of curing at 25ºC. Microstructural analyses of pastes were performed by powder X-ray diffraction (XRD), Fourier transform infrared spectroscopy (FTIR), thermogravimetric analysis (derivative DTG curves), mercury intrusion porosimetry (MIP) and field emission scanning electron microscopy (FESEM).

2. MATERIALS AND METHODS

2.1 Materials

The main material of this study is the sugar cane straw ash (SCSA). The straw was collected in a sugar cane plantation close to Ilha Solteira city (São Paulo, Brazil). Afterwards, it was transformed by means of an autocombustion process with a maximum combustion temperature of 700ºC, yielding a residual ash. Since this residue presents a certain amount of unburned particles, the ash was passed through sieves to remove them. Finally, the passed powder was milled in a ball mill for 50 minutes to reduce and homogenise the ash particles, and then the SCSA was ready to be tested. The blast furnace slag (BFS) was acquired from the Ribas do Rio Pardo (Mato Grosso do Sul, Brazil). The chemical composition of both SCSA and BFS are shown in Table 1. BFS showed the typical chemical composition: CaO, SiO_2 and Al_2O_3 were the main oxides. SCSA had SiO_2 as the main component (58.6%), and Al_2O_3 and Fe_2O_3 were also significant components. Regarding the particle size of the solid precursors, SCSA presents a mean particle diameter (D_{med}) and median particle diameter (D_{50}) of 18.1 μm and 10.6 μm, respectively; for the BFS, these values are 27.5 and 21.4 μm, respectively. In the alkaline solution preparation, sodium hydroxide (solid, 98% purity) and sodium silicate (solid, 18 wt% Na_2O, 63 wt% SiO_2) supplied by Dinâmica Química were used. For mortar preparation, natural sand with a fineness modulus of 2.05 and specific gravity of 2667 kg/m^3 was obtained from Castilho City (São Paulo, Brazil).

Table 1 – Chemical characterisation of the solid precursors utilised in this paper (BFS and SCSA)

Solid Precursor	SiO_2	Al_2O_3	Fe_2O_3	CaO	MgO	K_2O	SO_3	Cl	Others	LOI
SCSA	58.6	9.0	8.4	4.6	1.6	5.4	1.9	0.7	3.3	6.5
BFS	33.0	11.5	0.6	43.5	7.3	0.4	1.9	0.1	1.6	0.1

2.2 Alkali activated binders' dosage and preparation

In this study, six different alkaline solutions were prepared, in order to assess their influence on the mechanical properties of the designed AAM. The H_2O/Na_2O molar ratios assessed (called η) were 22, 28 and 37. For each η value, there were two SiO_2/Na_2O (called by ε) molar ratios evaluated in this study: 0 (only sodium hydroxide in the solution) and 0.75. Regarding the solid precursors, for the intermediary η ratio of 28, the BFS/SCSA proportions studied (y/z) to evaluate the influence of the ash in AAM systems were 100/0, 85/15, 75/25, 67/33 and 50/50. For the other η values (22 and 37), the BFS/SCSA proportions assessed were 100/0 and 75/25. Therefore, the total studied mixes in this paper was eighteen, as summarised in Table 2. In all mixes (pastes and mortars), the water/precursor ratio was maintained at a constant level of 0.45. For mortars, natural sand was added in the proportion solid precursor/sand of 1/2.5. The dosages nomenclature proposed in this study is η-ε-y/z and specimen names are also shown in Table 2.

Regarding the preparation of AAMs, first, the alkaline solution was prepared. Since the dissolution of sodium hydroxide in water releases heat, the resulting solution was left to reach room temperature. Afterwards, the solid precursor was mixed with the alkaline solution, until proper homogenisation was attained. For mortars, sand was finally added and mechanically stirred for 3 minutes. Pastes and mortars were cured at 25ºC and relative humidity higher than 95% until the tests age.

Table 2 – Mixture dosage and specimen´s names and tests carried out: compressive strength (Rc), X-ray diffraction (XRD), Fourier transform infrared spectroscopy (FTIR), Thermogravimetric analyses (TGA), Mercury intrusion porosimetry (MIP) and Field emission scanning electron microscopy (FESEM)

Specimen's name	H_2O/Na_2O molar ratio (η)	SiO_2/Na_2O molar ratio (ε)	BFS / SCSA (y/z)	Testing ages (days)					
				Rc	XRD	FTIR	TGA	MIP	FESEM
22-0-100/0	22	0	100/0	3-7-28-90	-	-	-	-	-
22-0-75/25			75/25		-	-	-	-	-
22-0.75-100/0		0.75	100/0	3-7-28-90	-	-	-	-	-
22-0.75-75/25			75/25		-	-	-	-	-
28-0-100/0	28	0	100/0	3-7-28-90	90	7-28-90	7-28-90	90	90
28-0-85/15			85/15		-	-	-	-	-
28-0-75/25			75/25		90	7-28-90	7-28-90	90	90
28-0-67/33			67/33		-	-	-	-	-
28-0-50/50			50/50		-	-	-	-	-
28-0.75-100/0		0.75	100/0		90	7-28-90	7-28-90	90	90
28-0.75-85/15			85/15		-	-	-	-	-
28-0.75-75/25			75/25		90	7-28-90	7-28-90	90	90
28-0.75-67/33			67/33		-	-	-	-	-
28-0.75-50/50			50/50		-	-	-	-	-
37-0-100/0	37	0	100/0	3-7-28-90	-	-	-	-	-
37-0-75/25			75/25		-	-	-	-	-
37-0.75-100/0		0.75	100/0	3-7-28-90	-	-	-	-	-
37-0.75-75/25			75/25		-	-	-	-	-

2.3 Test procedures for pastes and mortars

XRD patterns were accomplished by a Bruker AXS D8 Advance with a voltage of 40 kV, current intensity of 20 mA and a Bragg's angle (2θ) in the range of 5-70°. FTIR spectra were obtained by a Bruker Tensor 27 in the range of 400 and 4000 cm^{-1}. The DTG curves were carried out by a TGA Mettler-Toledo TGA 850, where the specimen was heated in a 70 μL alumina crucible in the temperature range of 35-1000ºC, with a heating rate of 20ºC.min^{-1} and air atmosphere (75 mL.min^{-1} gas flow). Mercury intrusion porosimetry (MIP) was carried out by a Micrometrics Instrument Corporation AutoPore IV 9500, using intrusion pressure from 6.6 kPa to 402.2 MPa, representing measurement diameter pores in the range of 222.2 μm and 3.6 nm. Finally, field emission scanning electron microscopy (FESEM) images were taken by a ZEISS Supra 55 in fractured surface sample covered with carbon in order to evaluate the gel structure and chemical composition. Some micrographs were taken by using an in-lens

system, which virtually eliminates aberrations, resulting in optimal spatial resolution; clearer and less electrostatically distorted images were recorded. XRD, FTIR, TGA, MIP and FESEM tests were carried out at different ages, according to Table 2.

Mortars were cast in a cubic mould of 50 x 50 x 50 mm^3 and tested in an EMIC Universal Machine with a load limit of 2000 kN. Compressive strengths of mortars were assessed after 3, 7, 28 and 90 days of curing at 25ºC and relative humidity (RH) was higher than 95% for all dosages studied.

3. RESULTS AND DISCUSSION

3.1 Compressive strength of mortars

Compressive strength results of mortars are summarised in Table 3. BFS mortars activated with $\varepsilon = 0$ (22-0-100/0, 28-0-100/0 and 37-0-100/0) showed the lowest strengths. At early ages (3 and 7 days), the mortar with the highest concentrated activating solution (22-0-100/0) yielded lower strengths than the other mortars activated with other NaOH solutions: this behaviour suggested that high sodium concentration did not have advantages in terms of early strength development. For longer curing times (28 and 90 days), all BFS mixes activated with NaOH yielded similar strength (25-33 MPa at 28 days and 34-36 MPa at 90 days). BFS samples activated with $\varepsilon = 0.75$ solution (22-0.75-100/0, 28-0.75-100/0 and 37-0.75-100/0) showed higher strengths when compared to mortars activated with $\varepsilon = 0$ solution. Thus, strengths reached after 7 days for $\varepsilon = 0.75$ systems were similar to those obtained for $\varepsilon = 0$ after 90 days of curing. This behaviour revealed the important role of sodium silicate in the activation of BFS. BFS mortars with $\varepsilon = 0.75$ yielded very high strengths after 28 and 90 days: 53-61 and 64-67 MPa, respectively.

Related to the influence of the partial replacement of BFS by the sugar cane straw ash (SCSA) in the AAM, specimens for all η values without the sodium silicate ($\varepsilon = 0$) showed a significant improvement compared to the corresponding ones with BFS and $\varepsilon = 0$. Thus, noticeably, strengths reached for samples with BFS/SCSA=75/25 (25% replacement of BFS) were in the range 50-57 MPa at 28 days and in the 56-59 MPa at 90 days. These values, compared to those obtained for BFS activated mortars with $\varepsilon = 0$, represent increasing mean values of 86% and 66%

at 28 and 90 days, respectively. These values were slightly lower than those found for BFS activated with $\varepsilon = 0.75$ solutions, which means that the role played by SCSA in the BFS/SCSA mixtures with $\varepsilon = 0$ was comparable to that for sodium silicate. Curiously, for the earliest curing age (3 days) the effect of the SCSA was negligible with $\varepsilon = 0.75$: for BFS/SCSA samples activated with $\eta = 22$ and $\eta = 28$ solutions; similar strengths to that found for BFS systems with $\varepsilon = 0$ were reached. In contrast, BFS/SCSA samples activated with $\eta = 37$ yielded only 1.9 MPa (BFS with $\varepsilon = 0$ sample yielded 13.4MPa), which means that the lowest sodium concentration solution was not very effective in the dissolution of reactive silica from SCSA at this age [22].

Specifically, for the BFS/SCSA with $\eta = 28$ samples, different replacement SCSA percentages were studied (15, 25, 33 and 50% replacements). The replacement interval of 25-50% mortars did not show a difference in the compressive strength values after 90 days of curing, being slightly superior to the 15% replacement. Additionally, the compressive strength development from the BFS/SCSA ratio of 75/25 presented better results than the 67/33 and 50/50 mixtures, since the results of the early curing times of that blend are significantly higher than these ones.

Regarding the specimens with sodium silicate ($\varepsilon = 0.75$), the BFS/SCSA 75/25 mixture presented slightly lower 90-day compressive strengths than the control ones for the three η values tested, which is different to that which occurred for the blends with $\varepsilon = 0$. However, for early curing ages, the strengths for SCSA-containing systems were significantly lower. This behaviour suggests that, at early ages, the dissolution of silica from SCSA and the presence of silicate anions in the solution have a negative effect on the strength development.

Again for the $\eta = 28$ mixtures, SCSA percentages in the range 15-33% presented better compressive strength development until the 90th day of the study, whereas 50% showed worse results than those. The presence of SCSA in mixtures with $\varepsilon = 0.75$ did not show any difference compared to the control one. From these compressive strength results, the optimal BFS/SCSA proportions are 75/25 and 67/33. Noticeably, the BFS/SCSA 50/50 sample did not set before 7 days of curing, which strengthens the proposed idea regarding the bad compatibility between SCSA and sodium silicate for a good early strength development [1]. In these cases, a large amount of silicate in solution is produced because the sodium silicate in the activator and the solubilisation of silica from SCSA by NaOH. In these

conditions, the silicate/BFS ratio was notably increased (especially for 50% replacement of BFS by SCSA) and the effective NaOH concentration for achieving BFS was drastically diminished [23].

Table 3 – Compressive strength of mortars (MPa) and their standard deviations

Specimen name	Compressive strength (MPa)			
	25ºC, RH > 95%			
	3 days	7 days	28 days	90 days
22-0-100/0	11.8 ± 0.2	16.5 ± 0.5	25.0 ± 1.1	35.7 ± 0.5
22-0-75/25	10.2 ± 0.2	29.0 ± 1.8	57.4 ± 0.4	58.8 ± 2.3
22-0.75-100/0	15.2 ± 0.1	33.1 ± 1.5	55.8 ± 4.3	67.2 ± 0.4
22-0.75-75/25	6.5 ± 0.1	23.3 ± 1.3	56.7 ± 0.7	62.1 ± 2.3
28-0-100/0	16.1 ± 0.7	21.4 ± 0.8	32.8 ± 1.2	34.7 ± 4.1
28-0-85/15	7.1 ± 0.1	18.1 ± 0.9	41.2 ± 2.2	50.0 ± 1.9
28-0-75/25	11.3 ± 2.4	26.9 ± 0.7	54.0 ± 1.0	57.0 ± 2.5
28-0-67/33	3.1 ± 0.1	9.5 ± 0.6	46.0 ± 4.2	57.2 ± 4.9
28-0-50/50	2.8 ± 0.1	3.2 ± 0.7	35.0 ± 0.1	57.3 ± 2.0
28-0.75-100/0	20.3 ± 1.1	36.2 ± 2.0	60.4 ± 4.8	64.5 ± 1.5
28-0.75-85/15	3.5 ± 0.1	17.1 ± 0.4	42.4 ± 1.9	65.6 ± 3.2
28-0.75-75/25	3.2 ± 0.2	13.6 ± 0.6	48.7 ± 4.0	63.6 ± 4.3
28-0.75-67/33	5.4 ± 0.1	18.5 ± 0.5	52.7 ± 0.7	63.1 ± 1.7
28-0.75-50/50	-	-	21.1 ± 0.5	50.4 ± 1.2
37-0-100/0	13.4 ± 0.1	19.0 ± 0.5	29.6 ± 0.7	36.0 ± 1.4
37-0-75/25	1.9 ± 0.0	12.3 ± 0.5	50.8 ± 1.1	56.6 ± 1.6
37-0.75-100/0	15.3 ± 0.9	33.0 ± 1.5	53.4 ± 2.1	64.2 ± 3.0
37-0.75-75/25	1.7 ± 0.1	10.7 ± 0.1	53.3 ± 1.3	58.6 ± 4.5

The use of sodium silicate ($\varepsilon = 0.75$) only showed beneficial results to the BFS/SCSA proportion of 100/0: for the all η values, the final compressive strength of this solid precursor proportion showed higher results when compared to those without sodium silicate. When BFS was partially replaced by SCSA, the use of sodium silicate did not favour the mortar strength development. The final compressive strength (90 days) of the mortars with sodium silicate is similar to those that do not have this reagent, and also negatively affected the mechanical strength development: the compressive strength of SCSA-mortars with $\varepsilon = 0$ showed higher compressive strength at early ages when compared to the specimens with the $\varepsilon = 0.75$ ones. Making an overview of all of the results, the comparison between the specimens with SCSA activated with only sodium hydroxide (SCSA percentages in the interval 15-50% and $\varepsilon = 0$) and those without SCSA activated with sodium hydroxide and silicate (SCSA percentage

of 0% and ε = 0.75) may be highlighted. In order to assess the importance of the SCSA contribution, and the possibility to compare their mortars with the control ones (BFS/SCSA=100/0) with sodium silicate, an φ ratio is proposed in this study. This φ parameter is the ratio between the compressive strength of a mortar with a certain BFS/SCSA proportion different than 100/0 (y/z, being 85/15, 75/25, 67/33 or 50/50), a determined η value and ε = 0 ($Rc_{\eta\text{-}0\text{-}y/z}$) over the control one (only BFS), with the same H_2O/Na_2O ratio and activated with sodium silicate solution (ε = 0.75) for the same curing time ($Rc_{\eta\text{-}0.75\text{-}100/0}$), as in Equation 1:

$$\varphi = \frac{Rc_{\eta-0-y/z}}{Rc_{\eta-0.75-100/0}} \qquad Eq.1$$

The φ values for 7, 28 and 90 days of curing are presented in Figure 1. After 7 days of curing, the specimen with η = 22 presented a compressive strength that was slightly lower than the control (22-0.75-100/0), and reached an φ value of 0.87. The sample 28-0-75/25 showed a lower rate of 0.74, whereas the other specimens presented φ ratios lower than 0.50. This behaviour can be explained by taking into account that the commercial sodium silicate was already dissolved in the aqueous medium, which means that the reaction process occurs faster than in the mortars with SCSA, leading to a higher compressive strength at early curing ages. On the other hand, after 28 days, the effect of SCSA in the development of the strength gained in importance: 22-0-75/25, 28-0-75/25 and 37-0-75/25 specimens showed φ values over than 0.80, indicating that the SCSA contribution as a silica source mainly occurred in the 7-28 days of curing period. For this curing time, it is highlighted that the 22-0-75/25 reached compressive strength slightly above the control, since the φ value of this mortar was 1.04. The higher amount of Na^+ was shown to be beneficial in the first 28 days of curing, because this mortar presented a compressive strength similar to the control and φ values always over 0.80. Regarding the SCSA content, the mortars with η = 28 showed that the optimum replacement was 25%, due to the highest φ value for 28-0-75/25 system (φ=0.89) at this curing age. After 90 days of curing, all mortars showed φ values in the range from 0.80-0.90, confirming that the SCSA can be used as a silica source in alkali-activated binders based on BFS. Interestingly, for BFS/SCSA = 75/25 systems, the values of φ over 0.75 at 90 days confirm that the use of SCSA is interesting from two points of view: the partial replacement of BFS and the total replacement of sodium silicate. At this curing time, neither the quantity of Na^+ nor the percentage of SCSA utilised in the mortar had a significant affect.

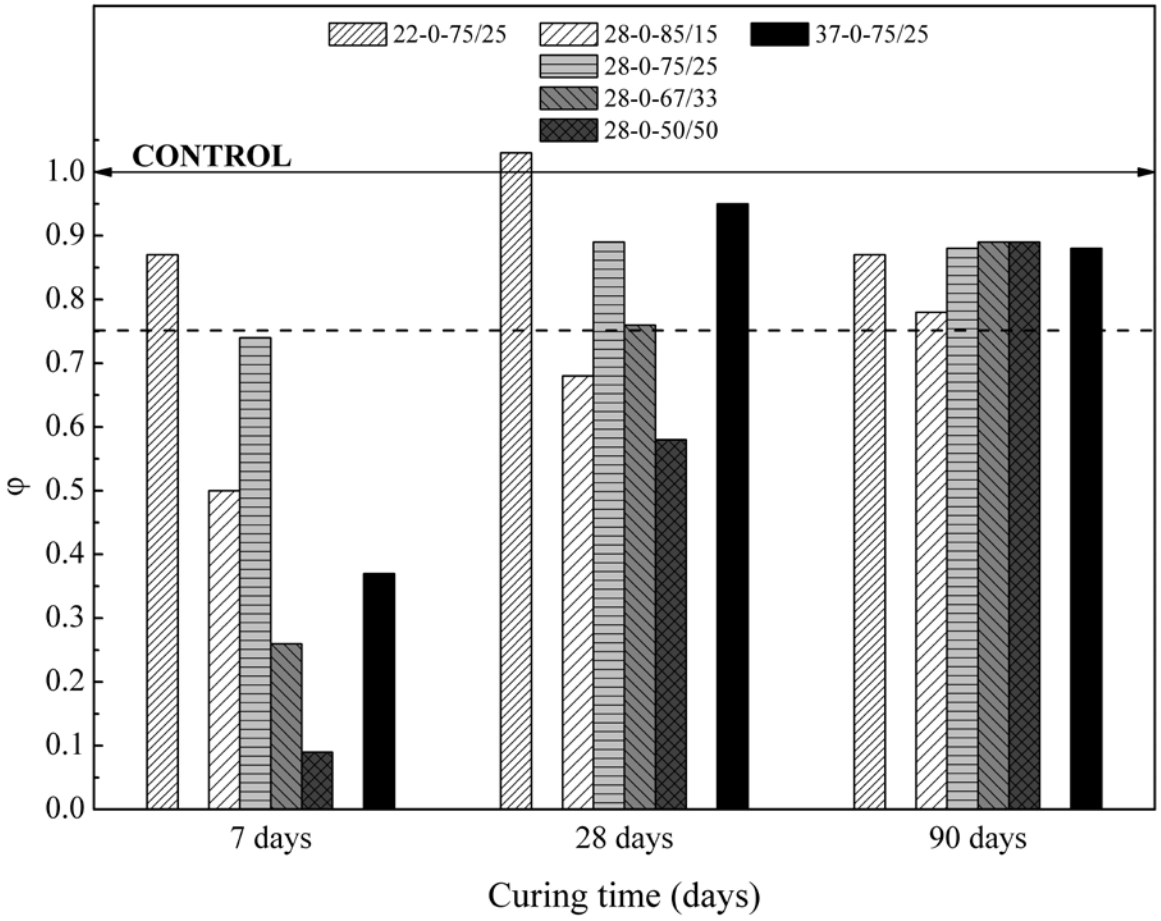

Figure 1 – Values of the φ ratio for mortars containing SCSA at 7, 28 and 90 days of curing

3.2 Microstructural studies

XRD patterns of the raw materials (BFS and SCSA) and the pastes 28-0-100/0, 28-0-75/25, 28-0.75-100/0 and 28-0.75-75/25 after 90 days of curing are shown in Figure 2. Firstly, regarding the raw materials BFS and SCSA, XRD patterns show a baseline deviation in the Bragg's Angle range of 17-33º and 20-35º, respectively, which is characteristic of the presence of amorphous phases. The presence of an important amount of quartz (PDF Card #331161) in SCSA meant that this baseline deviation was only easily identified by enlargement of the diffractogram in the 20-35º range. In addition, calcite (PDF Card #050586) was present in the ash. Regarding XRD patterns of pastes, a baseline deviation in the 2θ range of 22-38º was observed in all cases. This behaviour was observed in

other studies of the alkaline activation of BFS [1,6]. The XRD pattern for 28-0-100/0 showed the strongest broad peak centred at 29.32º and a broad weaker peak at 32.08º, which can be associated with the presence of C-S-H gel (probably this gel has sodium and aluminium, (C,N)-A-S-H phase); additionally, the peak from calcite in the very close 2θ value of 29.32º overlapped. The presence of calcite in this sample was confirmed by the identification of other related peaks: 22.97, 35.93, 43.09, 47.39, 48.44 and 57.35º. This calcite was due to the slight carbonation of the sample, according to the results from thermogravimetric analysis. A small quantity of quartz was also identified, which comes from the BFS, suggesting that this crystalline phase did not react in the process after 90 days of curing. Finally, minor phases were also identified: hydrotalcite ($Mg_6Al_2CO_3(OH)_{16}.H_2O$, PDFcard 140191) and katoite ($Ca_3Al_2(SiO_4)(OH)_8$, PDFcard 380368). The XRD pattern for 28-0.75-100/0 was similar to the above-described sample without sodium silicate, suggesting that the nature of the crystalline phases was not influenced by the nature of the chemical activator. For samples containing SCSA (28-0-75/25 and 28-0.75-75/25), the main peak belonged to quartz phase, suggesting that this crystalline phase did not react towards the alkaline medium. Similar peaks to BFS-containing pastes were identified: calcite and (C,N)-A-S-H. This means that the nature of the crystalline products did not strongly influence the hydration of BFS by the presence of SCSA.

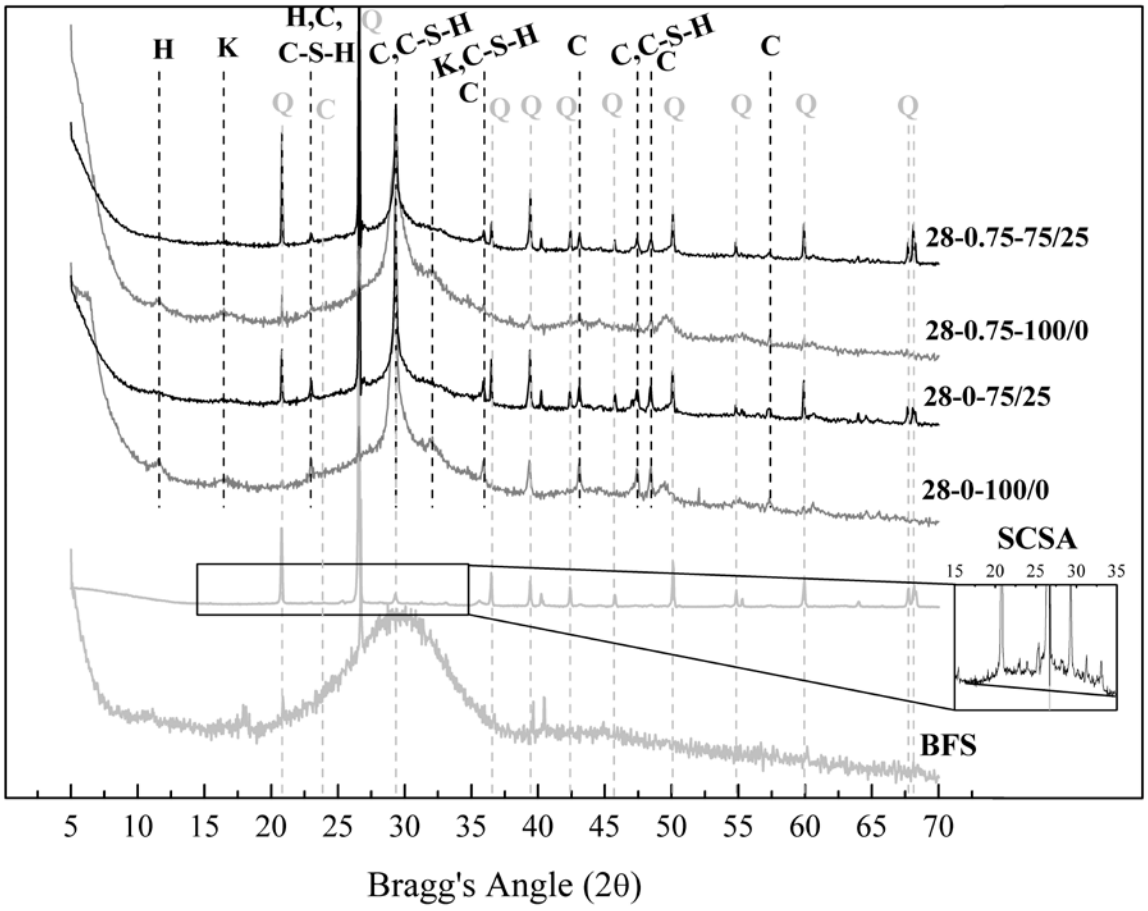

Figure 2 – XRD patterns of the raw materials (BFS and SCSA) and the pastes 28-0-100/0, 28-0-75/25, 28-0.75-100/0 and 28-0.75-75/25 after 90 days of curing (Key: Q: quartz; C: calcite, H: hydrotalcite; K, katoite; C-S-H: calcium silicate hydrate)

FTIR spectra of the raw materials (BFS, SCSA and a BFS/SCSA mixture by proportion of 75/25 before combining with the alkaline solution) and the pastes 28-0-100/0, 28-0-75/25, 28-0.75-100/0 and 28-0.75-75/25 after 7, 28 and 90 days of curing are shown in Figure 3. The broadband in the range from 800-1270 cm^{-1} may be highlighted, as this is related to the amorphous Si-O-T vibrations of the raw materials and pastes (being T Si or Al) [6,24]. Firstly, regarding the raw materials, the BFS spectrum presented a broadband centred at 964 cm^{-1}; the SCSA spectrum also showed a broadband, in this case centred at 1032 cm^{-1}. A blend of BFS/SCSA was also assessed in order to visualise the modification on the spectrum when raw materials are combined with the alkaline solution before the reaction. In this case, the broadness of the band was much larger than those for raw materials (from 810 to 1270 cm^{-1}) as a

consequence of the sum of absorptions from both materials. This more flattened broadband must be taken as the starting point for monitoring the hydration evolution by FTIR.

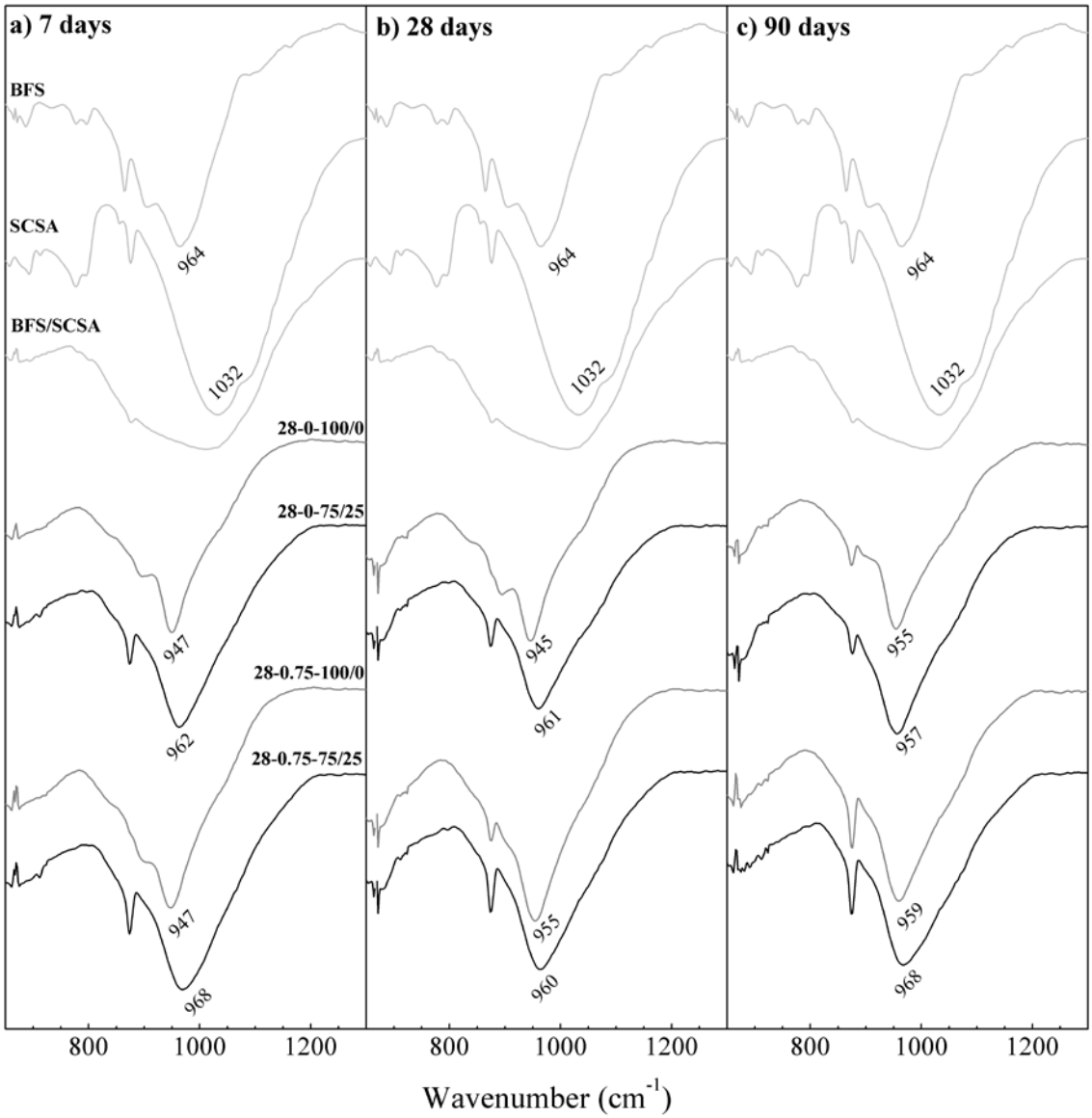

Figure 3 – FTIR spectra of the raw materials (BFS and SCSA) and the pastes 28-0-100/0, 28-0-75/25, 28-0.75-100/0 and 28-0.75-75/25 after 7, 28 and 90 days of curing

Regarding the AAM pastes after 7 days of curing (Fig. 3a), it can be seen that the strongest peaks are in the interval of 940-970 cm^{-1}, which is the wavenumber region for the (C,N)-A-S-H gels from the BFS activation [6, 24]. The changes observed in the band position for both BFS and BFS/SCSA systems can be related to the effect of Al/Si and Ca/Si ratios: the decrease of these values induces an increase in the wavenumber band [25,26]. As the aluminium content for both raw materials is very low, the changes in the wavenumbers is more related to changes in the Ca/Si ratio. In addition, the dissolution of silica-glassy part from SCSA (whose band absorption was higher in energy than the one found for gel) that reacts with BFS particles and forms part of the gel can also shift the broadband position to a lower wavenumber. In general, for BFS samples, the broadband peak energy increased with curing time, with this increase being higher for sodium silicate activated paste (28-0.75-100/0). This suggests that silicate tetrahedral anions are more strongly linked in the (C,N)-A-S-H gel. On the contrary, BFS/SCSA samples did not show a significant shift to higher energy in the broadband FTIR peak with curing time. This behaviour can be explained as follows: despite the formation of a more linked structure with the presence of SCSA (as suggested by compressive strength behaviour), part of glassy silica from SCSA was reacted to form cementing gel. In this way, the intensity of the absorption related to SCSA was diminished, and the resulting peak of the overlapped absorptions from the unreacted SCSA and the formed gel did not shift to higher energies. In the case of BFS specimens (without SCSA), the difference between the main peak of raw material (964 cm^{-1}) and the peak associated with the formed gel (945-959 cm^{-1}) in the activated pastes was very low; the influence of the raw BFS consumed through the reaction was negligible in the FTIR absorption overlap. The absorption band related to the presence of carbonates (875 cm^{-1}) was easily identified in SCSA and in all pastes which contain this ash. This FTIR peak increased with curing time, suggesting the carbonation of the pastes during the curing process. This carbonation process also affected the BFS pastes. Thus, after 7 days of curing, the peak centred at 875 cm^{-1} was not shown for 28-0-100/0 and 28-0.75-100/0 pastes; however, after 28 curing days, paste activated by sodium silicate showed this peak, and both pastes showed this absorption peak after 90 curing days.

TGA results (derivative thermogravimetric curve, DTG) on the pastes 28-0-100/0, 28-0-75/25, 28-0.75-100/0 and 28-0.75-75/25 after 7, 28 and 90 days of curing are presented in Figure 4. In this study, the main peaks and most important mass losses were at the temperatures of 110-165, 200-250 and 580-620ºC. Therefore, Table 4 is presented with the mass losses in the following important temperature ranges of 35-250ºC (P_g, mass loss related to the formed

gel), 450-650ºC and the total mass loss (P_t) obtained in the test (35-1000ºC). DTG peaks in the range 110-160ºC are related to the dehydration of (C,N)-A-S-H or C-S-H gels from the activation of the BFS [6,13,27]. The peak placed at 200-250ºC is associated with the decomposition C-A-S-H gels (e.g. stratlingite or C_2ASH_8) [6,13,28]. Finally, the peaks observed in the range of 580-600ºC are related to the decomposition of calcium carbonate. This decomposition temperature range is noticeably lower than that observed for calcite from natural source (700-850ºC): this is probably due to the particle size of the $CaCO_3$ crystals produced in the carbonation process, which is a poorly crystallised phase [27] and to the presence of sodium ions, both influencing the decrease in temperature decomposition.

In general terms, it can be noticed that the mass losses increased with curing time, and for a given curing age, they increased with the presence of SCSA and/or sodium silicate: 28-0-100/0 presented the lowest total mass loss, and also presented the lowest mass losses for the ranges 35-250 and 450-650ºC. For early age SCSA-containing samples (7 days), the peak centred in the range from 450-650ºC was very intense, as can be seen in DTG curves (Figure 4). This was probably due, on the one hand, to the initial calcium carbonate present in the ash, as confirmed by XRD, and on the other hand by the higher carbonation rate of the sample with the presence of SCSA. For medium curing times (28 days), sample 28-0.75-100/0 also showed this peak, and the same long curing time (90 days) was seen in the 28-0-100/0 sample. These results suggest that the formation of the compound that decomposes at this temperature range is formed in all of the studied systems; however, the rate of formation changed depending on the mixture.

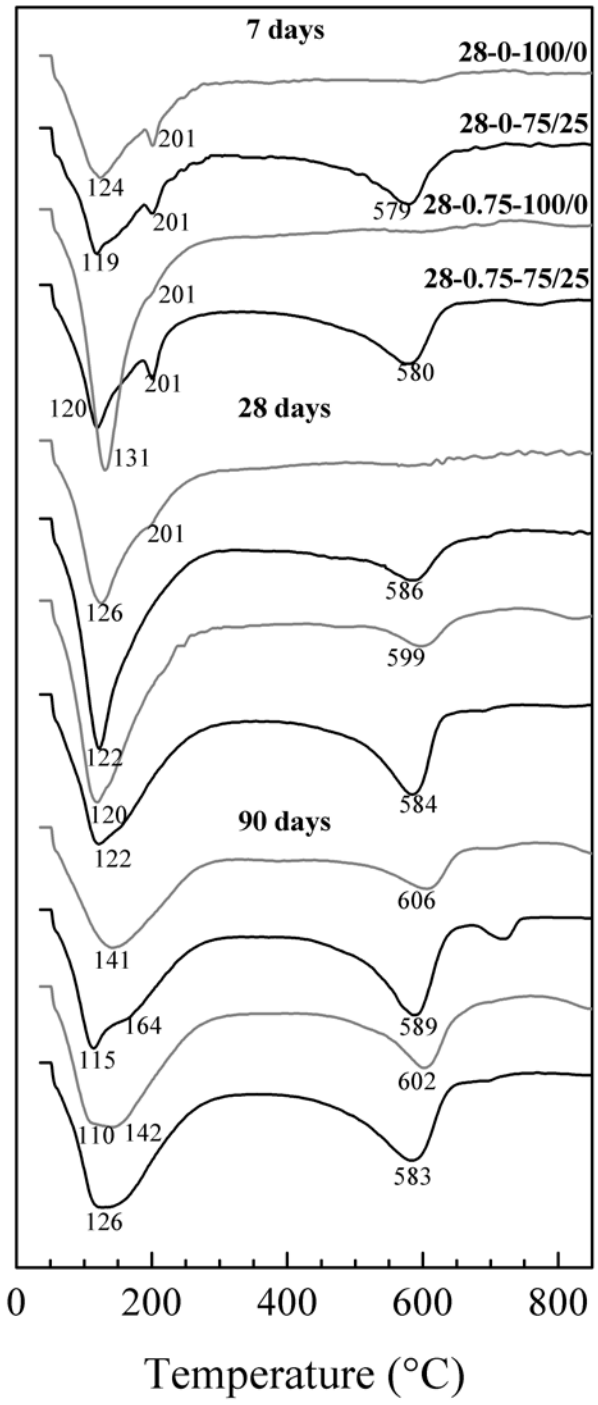

Figure 4 – DTG curves of the pastes 28-0-100/0, 28-0-75/25, 28-0.75-100/0 and 28-0.75-75/25 after 7, 28 and 90 days of curing

Table 4 – Mass losses (%) for the pastes 28-0-100/0, 28-0-75/25, 28-0.75-100/0 and 28-0.75-75/25 after 7, 28 and 90 days of curing at different temperature ranges (35-250ºC, 450-650ºC, and total mass loss 35-1000ºC).

Specimen	Mass losses (%)								
	7 days			28 days			90 days		
	35-250 ºC (P_g)	450-650 ºC	Total (P_t)	35-250 ºC (P_g)	450-650 ºC	Total (P_t)	35-250 ºC (P_g)	450-650 ºC	Total (P_t)
28-0-100/0	6.70	1.50	10.94	7.74	0.93	10.39	6.92	3.16	13.06
28-0 -75/25	6.20	3.57	12.05	9.96	3.36	16.03	7.69	5.37	15.78
28-0.75-100/0	10.14	1.03	13.33	10.25	2.44	15.30	8.85	4.18	15.95
28-0.75-75/25	6.47	3.99	12.79	8.23	4.72	15.30	8.73	5.45	17.11

Linear relationships have been found between the mass loss calculated from the thermogravimetric analysis and the developed compressive strength of mortar (Figure 5). As a consequence of the alkaline activation reaction progress, more hydrates are formed and more strength is developed. Thus, mass loss in the range 35-250ºC (P_g, related to low temperature water releasing from cementing gel) increased with compressive strength. A similar trend was found for total mass loss (P_t, in the range 35-1000ºC).

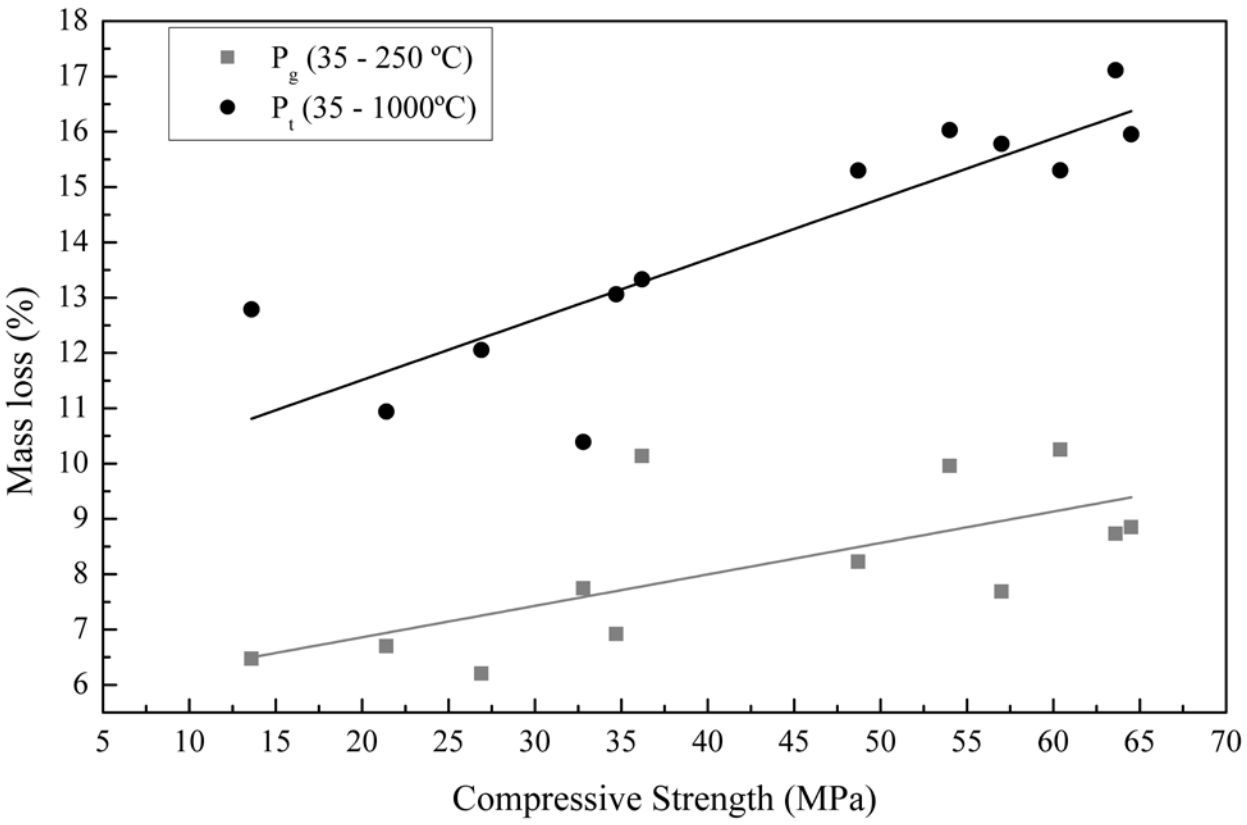

Figure 5 – Relationships between thermogravimetric mass losses for pastes (P_g, 35-250ºC; and P_t, 35-1000ºC) and the compressive strength of mortars.

MIP results for the pastes 28-0-100/0, 28-0-75/25, 28-0.75-100/0 and 28-0.75-75/25 after 90 days of curing are summarised in Table 5. The influence of SCSA in total porosity was insignificant for pastes activated with only sodium hydroxide (28.42 and 28.44% for 28-0-100/0 and 28-0-75/25, respectively); however, for the specimens with $\varepsilon = 0.75$, the paste with the ash presented greater porosity than its respective control (24.28 and 27.66% for 28-0.75-100/0 and 28-0.75-75/25, respectively). Taking into account the Hg retained in the intrusion-extrusion cycle, the presence of SCSA reduced the tortuosity in the paste from their respective controls (35.15 and 43.52%, respectively for $\varepsilon = 0$, and 27.85 and 38.75% for $\varepsilon = 0.75$, in that order). Probably, the presence of a fine powder (finer than BFS) and the production of cementing gel from its solution-precipitation process, yielded a more homogeneous capillary and gel pore networks, with the lower formation of ink-bottle pores.

Regarding the volume pore distribution of the pastes, differential and accumulated distribution MIP curves are depicted in Figure 6. Differential distribution curves (Figure 6a) showed two main types of pores for all tested pastes: capillary pores in the 100 to 5000 nm range (similar to large capillary pore network defined by Mindness et al. [29]) for OPC pastes, and small capillary and gel pores in the range 3 to 30 nm. Interestingly, SCSA containing pastes showed a low volume of Hg intruding into the highest size pores, being lower than 0.02 mL/g of paste (see Table 5). Contrarily, for samples without SCSA, this value was higher than 0.04 mL/g of paste. This means that SCSA reacted in the alkaline medium and produced a refined pore size in this range. This pore refinement produced smaller pores, and the intruded Hg volume was significantly higher for these smaller pores: in this way, the median pore diameter for SCSA containing AAMs was very low (9.14 and 7.04 nm for $\varepsilon = 0$ and $\varepsilon = 0.75$ respectively). Interestingly, the presence of the sodium silicate in the activated BFS sample (28-0.75-100/0) produced a beneficial effect on the reduction of porosity, and gel pore volume was very low compared to the other pastes. Probably, the presence of dissolved silicate in the activating solution favoured the formation of a denser gel with a gel pore size lower than 3 nm. This is the reason for the high mean diameter in volume (diameter of the pore size for which 50% of Hg volume was intruded): the value of 272 nm was due to the low gel pore volume. Thus, for silicate-activated BFS mortar, good mechanical properties were achieved.

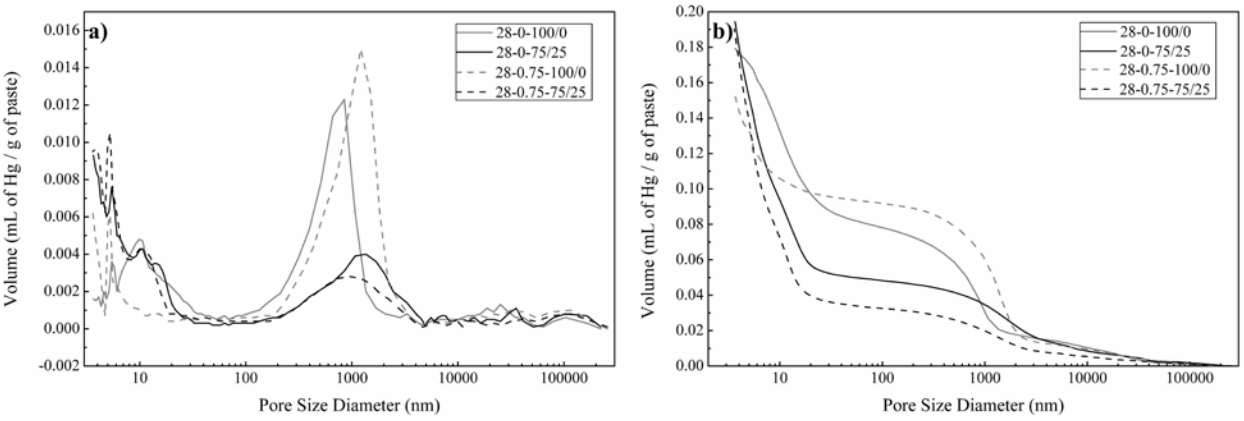

Figure 6 – MIP curves of the pastes 28-0-100/0, 28-0-75/25, 28-0.75-100/0 and 28-0.75-75/25 after 90 days of curing: a) differential, and b) accumulated distribution

Table 5 – MIP results of the pastes 28-0-100/0, 28-0-75/25, 28-0.75-100/0 and n8-0.75-75/25 after 90 days of curing

Specimen	Total porosity (%)	Total pore area (m^2/g)	Median pore diameter		Volume (mL of Hg/g of paste) and percentage volume			Hg retained (%)
			Volume (nm)	Area (nm)	> 5000 nm	5000 - 100 nm	< 100 nm	
28-0-100/0	28.42	43.06	27.04	7.62	0.0139 (7.74%)	0.064 (35.67%)	0.1013 (56.54%)	43.52
28-0-75/25	28.44	91.44	9.14	5.12	0.0126 (6.39%)	0.0355 (17.98%)	0.1463 (74.06%)	35.16
28-0.75-100/0	24.28	42.99	545.80	5.02	0.0118 (7.63%)	0.0801 (51.55%)	0.0633 (40.82%)	27.85
28-0.75-75/25	27.66	102.15	7.04	5.06	0.0072 (3.77%)	0.0254 (13.33%)	0.1578 (82.9%)	38.75

FESEM images of the pastes 28-0-100/0, 28-0-75/25, 28-0.75-100/0 and 28-0.75-75/25 after 90 days of curing are presented in the Figures 7-10. Regarding the paste with NaOH-activated BFS (28-0-100/0, Fig. 7), a particle of the solid precursor can be observed (BFS, spot A in Fig 7a) with some binding gel products (spot B, Fig 7a) around it. EDS analysis on the unreacted BFS particle gave the following atomic ratios: Ca/Si=0.76, Al/Si=0.33 and Na/Si=0.02. Most of the sample was occupied by the porous gel shown in the Fig 7b: it was formed by an imbricated set of irregular gel particles with sizes in the 200-50nm range. This gel was analysed by EDS, resulting in the following atomic ratios: Ca/Si = 0.83 ± 0.05, Al/Si = 0.34 ± 0.02, and Na/Si = 0.39 ± 0.06. The Si:Al:Ca proportion was 0.46:0.14:0.38, which corresponds to a C-A-S-H gel according to Abdalqader et al. [27]. FESEM micrographs taken by using an in-lens system (Fig 7c) showed a very homogeneous binding gel, and some small areas are covered by a denser gel (spot C, Fig 7d).

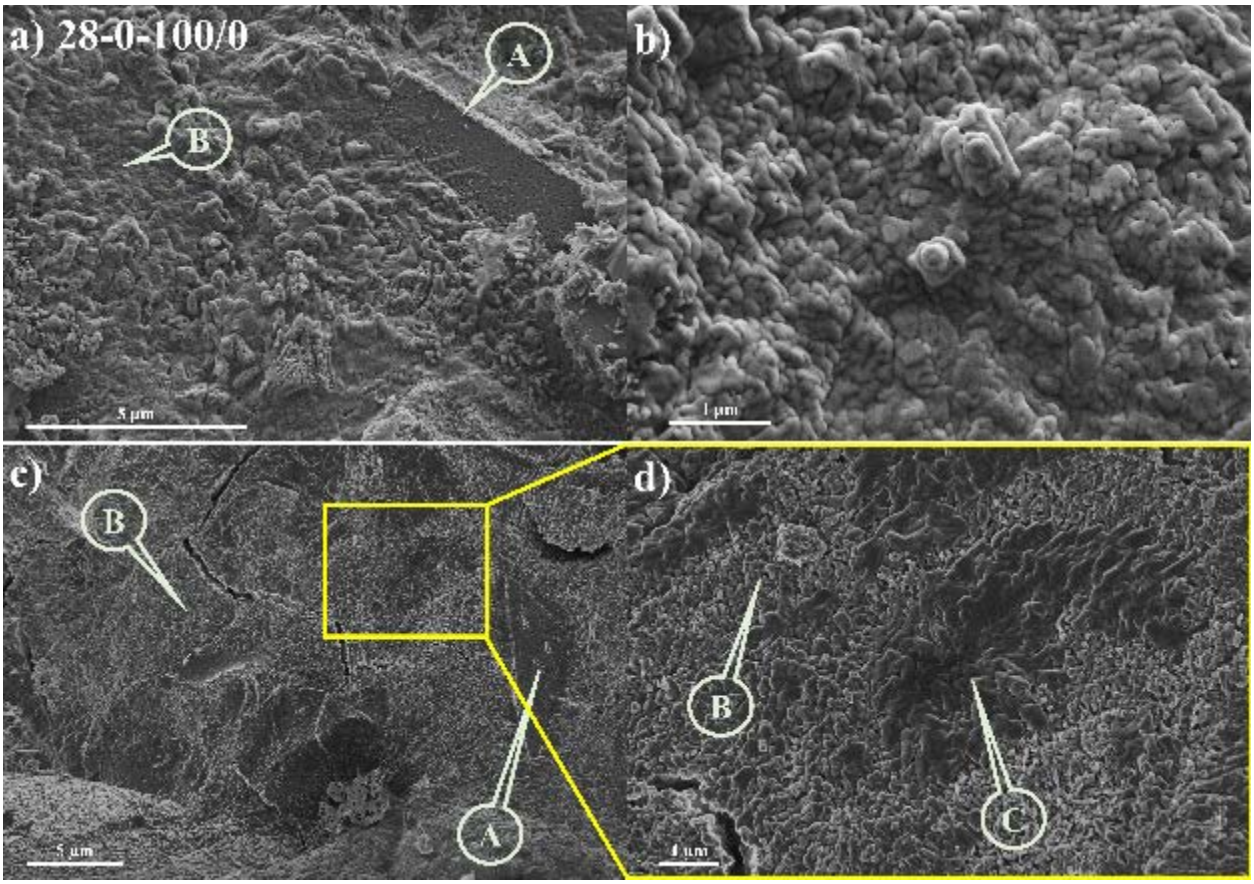

Figure 7 – FESEM micrographs of BFS activated paste with NaOH (28-0-100/0): a) general view of the paste with an unreacted BFS particle (spot A) and gel (spot B); b) detailed view of the gel; c) in-lens micrograph showing BFS unreacted particle (spot A) and main gel (spot B); d) enlarged zone from c), in which a denser gel is shown (spot C).

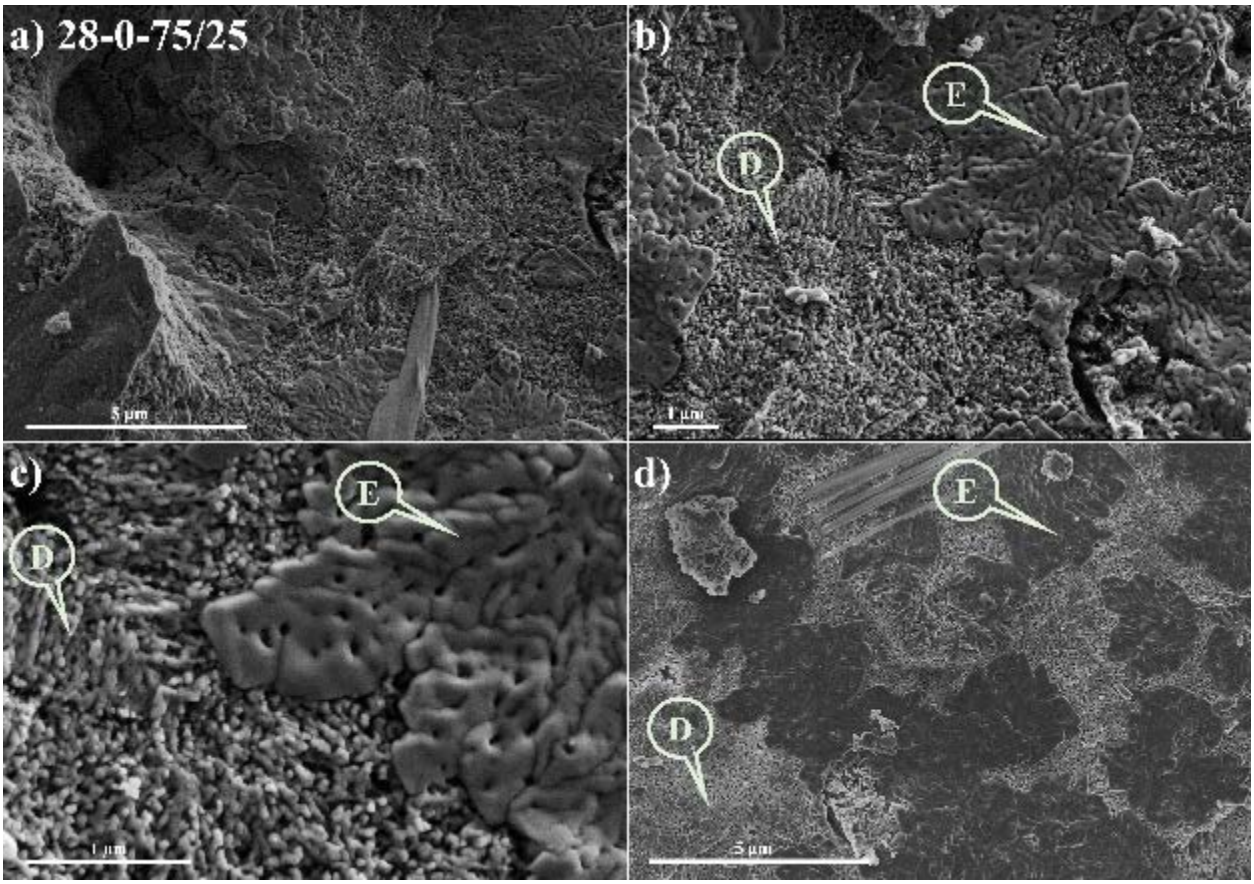

Figure 8 – FESEM micrographs of BFS/SCSA activated paste with NaOH (28-0-75/25): a) general view of the paste; b) general view of formed gels (spot D shows a porous gel, and spot E, a compacted gel); c) detailed view of both gels; d) in-lens view (lighter area for porous gel, and darker are for compacted gel).

In Figure 8, some FESEM micrographs for 28-0-75/25 paste are depicted. In Figure 8a, a general view of the gel is presented. In figures 8b and 8c, the presence of two different types of formed gels is noteworthy (see spots D and E). In spot D, the gel appears to be made of small particles (size under 50 nm), which are smaller than those obtained in the 28-0-100/0 specimen. In addition, its composition shows similar values to that obtained for porous gel in the 28-0-100/0 paste: Ca/Si = 0.84 ± 0.03, Al/Si = 0.28 ± 0.02, and Na/Si = 0.37 ± 0.04. In this case, the Si:Al:Ca proportion was 0.47:0.13:0.40, which also corresponds to a C-A-S-H gel. The Na/Si atomic ratio was similar to 28-0-100/0 paste (0.37 vs 0.39) despite the higher quantity of Si in the 28-0-75/25 paste due to the presence of SCSA. In contrast, the other gel (see spot E) showed a different morphology: more compacted, denser particles larger than 200 nm and irregularly hollowed (holes smaller than 50 nm size). This gel resulted in the following atomic ratios:

Ca/Si = 0.65 ± 0.08, Al/Si = 0.28 ± 0.02, and Na/Si = 0.30 ± 0.05. The Si:Al:Ca proportion was 0.52:0.14:0.34, which corresponds to a C(N)-A-S-H gel according to Abdalqader et al. [27]. The presence of SCSA in the mix favoured the formation of gels with a lower percentage of Ca and higher percentage of Na. Additionally, if the Na/Ca and (Na+K)/Ca ratios are compared, the influence on the composition of the gel can be noticed due to the K contained in the ash. Thus, the Na/Ca and (Na+K)/Ca ratios for 28-0-100/0 were very similar: 0.47 ± 0.06 and 0.52 ± 0.06 respectively. In contrast, gels in 28-0-75/25 paste showed much higher values for (Na+K)/Ca than for Na/Ca (for porous gel, 0.59 ± 0.01 vs. 0.44 ± 0.03; for compacted gel, 0.69 ± 0.12 vs. 0.47 ± 0.13). Figure 8d shows the distribution of both gels, porous and compacted, taken by using an in-lens system: darker zones belong to compacted gels and lighter ones to porous gels.

Regarding the specimen of BFS activated with both sodium hydroxide and silicate, Fig. 9a shows a general view of the microstructure, in which a large zone is covered by a compacted gel (spot G) with a smaller area covered by a more porous gel (spot F). Both types of formed gel can also be seen in the enlarged zone (Fig 9b). The porous gel (see spot F, Fig 9b) is similar to porous gel found in the microstructure of the 28-0-75/25 paste; the denser gel (see spot G, Fig 9b) is a continuous gel similar in composition to the one found in 28-0-75/25 paste (spot D). Also, some crystalline formations have been found: in Fig 9c, sheet-like crystals which were surrounded by a porous gel with the following composition (atomic ratios): Ca/Si = 0.85 ± 0.03, Al/Si = 0.29 ± 0.01, and Na/Si = 0.09 ± 0.03. This chemical composition suggested that this phase is a C-A-S-H gel, and probably the crystals are stratlingite, $Ca_2Al_2(SiO_2)(OH)_{10}\cdot 2.5H_2O$. In Fig 9d, some well-formed crystals, with a size of around 500 nm, were found. It was very difficult to perform chemical analysis because of the influence of the surrounding matrix, but interestingly the Na/Ca atomic ratio was very high (1.20 ± 0.02). This atomic ratio and the carbonation [30] of the sample (accordingly to TGA studies) allowed us to conclude that they are pirssonite, $Na_2Ca(CO_3)_2\cdot 2H_2O$. They can be formed due to carbonation of the sample.

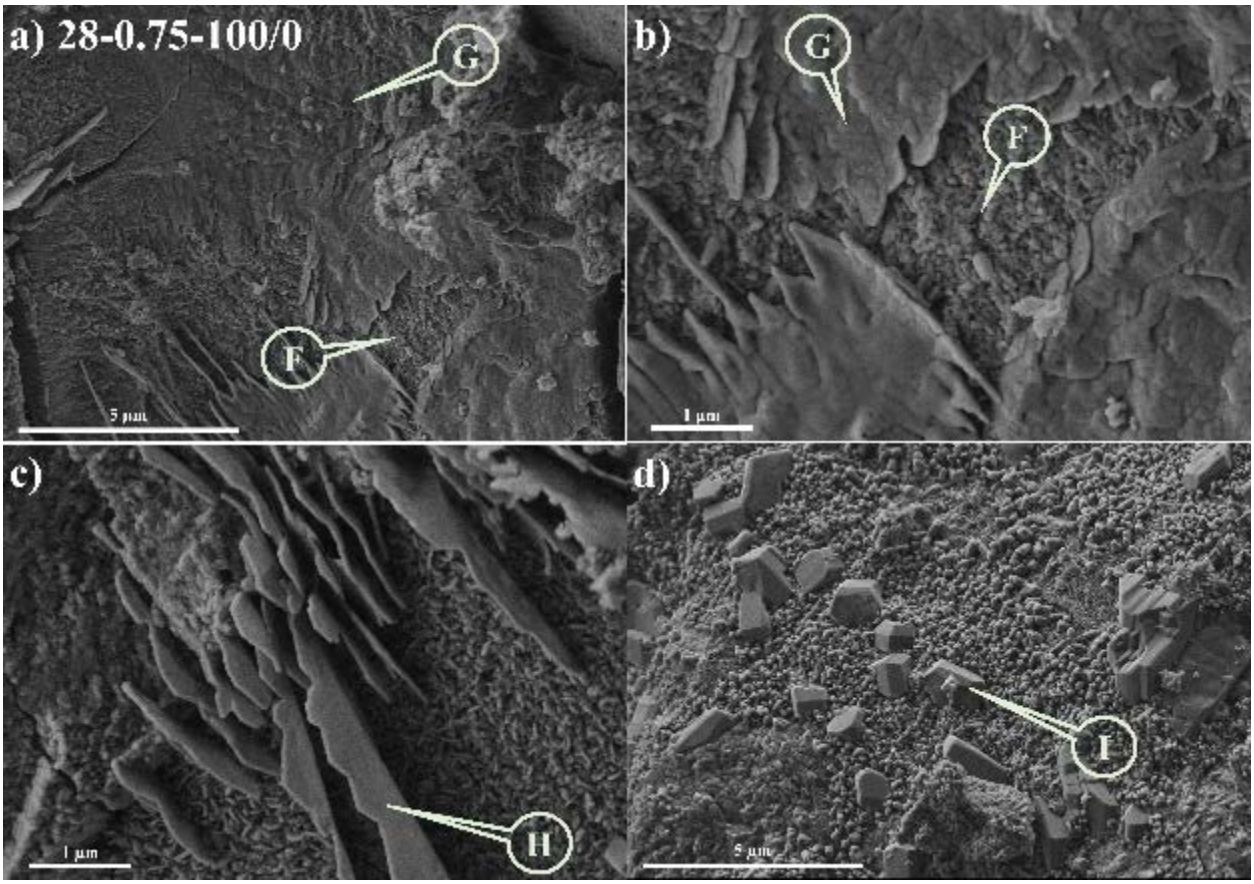

Figure 9 – FESEM micrographs of BFS activated paste with NaOH and sodium silicate (28-0.75-100/0): a) general view of the paste with some gel formation (spot F shows a porous gel, and spot G, a compacted gel); b) detailed view of formed gels; c) detailed view of sheet-like crystals (spot H, stratlingite); d) pirssonite crystals surrounded by gels.

In Fig. 10, some micrographs of the 28-0.75-75/25 paste are depicted. Fig 10a show a general view of the microstructure, in which much of the shown area is covered by a compacted gel (spot J). In the bottom-right corner of this micrograph, a particle of quartz was identified (probably from the SCSA, spot K). Figures 10b and 10c showed a detailed arrangement of the compacted gel (spot J): this gel was very similar to the compacted gel found for 28-0 -75/25 paste (see Fig 8c, spot D), in this case with a less hollowed pattern. Finally, in Fig 10d, pirssonite crystals (2-3 µm size) are shown, produced by the carbonation process.

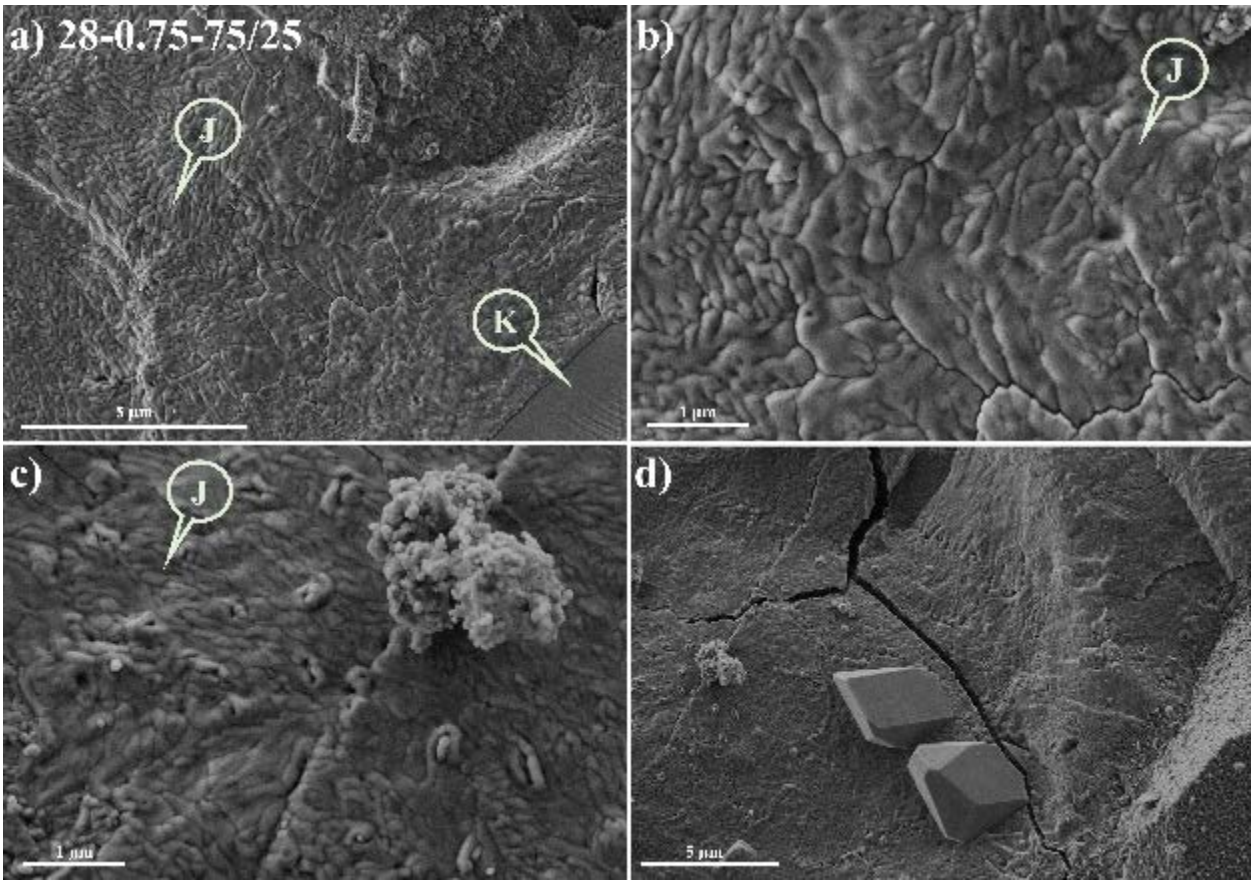

Figure 10 – FESEM micrographs of BFS/SCSA activated paste with NaOH and sodium silicate (28-0.75-75/25): a) general view of the paste with some gel formation (spot J) and a quartz particle (spot K); b) detailed view of compacted gel; c) detailed view of gel; d) pirssonite crystals surrounded by gels.

4. CONCLUSIONS

BFS alkali activated materials (AAM) activated by alkaline solutions in the H_2O/Na_2O (η) range of 22 to 37 (equivalent to a Na^+ molality of 5 to 3 $mol.kg^{-1}$) and the corresponding systems with the replacement of BFS by sugarcane straw ash (SCSA) were studied. NaOH and a mixture of NaOH+sodium silicate solutions, SiO_2/Na_2O ratios (ε) of 0 and 0.75 respectively, were assessed as activating solutions. In terms of mortar compressive strength behaviour, the replacement of BFS by SCSA did not negatively affect the mechanical performance produced. Interestingly, this replacement enabled the strength behaviour respect to the NaOH activated BFS-AAM: increases in the strength were 86% and 66% at 28 and 90 days, respectively. Moreover, these strength values were slightly

lower than those obtained for sodium silicate BFS-AAMs (at 90 days of curing, reached 80-90% of the strength for BFS-mortar). Also, the strength behaviour due to the influence of SCSA content (assessed on the interval of 15-50% replacement of BFS) did not show differences at 90 days of curing, which represents an interesting advantage in terms of the design and dosage of the AAMs. The optimum BFS/SCSA proportion was 75/25 due to its better compressive strength developed in the early curing time with respect to other tested replacements. Regarding the effect of the alkaline solution, the η ratio also did not influence the compressive strength at 90 days of curing; however, the strength evolution was significantly affected by the replacement: very early aged (3 days) mortars containing SCSA yielded low strength values. From microstructural studies, the significant role of SCSA in the development of the gel formed due to the alkali activation process was investigated. From XRD, TG and FTIR analyses, no differences in the nature of the cementing gel were found between the tested pastes. However, mercury intrusion porosimetry (MIP) measurements highlighted the critical reduction in the capillary pore volume for SCSA-containing pastes compared to the NaOH-BFS activated system. The high gel pore volume from MIP and the presence of compacted gel identified by FESEM in the SCSA systems agreed with the good mechanical behaviour of SCAS-activated mortars. A high proportion of a C(N)-A-S-H compacted gel was observed in these SCSA-systems, in a similar way to the observations for BFS activated with sodium silicate. From a general point of view, despite the low alkali concentration in the activation solutions, the SCSA plays an important role in the development of the binding ability of the alkali-activated paste. For these systems, a replacement of sodium silicate in the activating solution by the dosage of SCSA in the precursor can be proposed as a way to yield highly sustainable binders. Thus, interesting mixtures containing SCSA can be designed, which yield a similar performance to BFS systems, meaning that good valorisation of this biomass waste can be carried out for low alkalinity-activated materials.

ACKNOWLEDGMENTS

The authors would like to thanks to CNPq processo nº 401724/2013-1 and the “Ministerio de Educación, Cultura y Deporte” of Spain (“Cooperación Interuniversitaria” program with Brazil PHB-2011-0016-PC). Thanks are also given to the Electron Microscopy Service of the Universitat Politècnica de València.

REFERENCES

[1] J.C.B. Moraes, M.M. Tashima, J.L. Akasaki, J.L.P. Melges, J. Monzó, M.V. Borrachero, L. Soriano, J. Payá, Increasing the sustainability of alkali-activated binders: the use of sugar cane straw ash (SCSA), Constr. Build. Mater. 124 (2016) 148-154.

[2] J.M. Paris, J.G. Roessler, C.C. Ferraro, H.D. DeFord, T.G. Townsend, A review of waste products utilized as supplements to Portland cement in concrete, J. Clean. Prod. 121 (2016) 1-18.

[3] J. Payá, J. Monzó, M.V. Borrachero, M.M. Tashima, Reuse of aluminosilicate industrial waste materials in the production of alkali-activated concrete binders. In: F. Pacheco-Torgal, J.A. Labrincha, C. Leonelli, A. Palomo, P. Chindaprasirt, Handbook of Alkali-activated Cements, Mortars and Concretes, first ed. Cambridge, Woodhead Publishing and Elsevier, Waltham, Kidlington, 2015.

[4] M.O. Yusuf, M.A.M. Johari, Z.A. Ahmad, M. Maslehuddin, Evolution of alkaline activated ground blast furnace slag–ultrafine palmoil fuel ash based concrete, Mater. Des. 55 (2014) 387-393.

[5] A. Islam, U.J. Alengaram, M.Z. Jumaat, I.I. Bashar, The development of compressive strength of ground granulated blast furnace slag-palm oil fuel ash-fly ash based geopolymer mortar, Mater. Des. 56 (2014) 833-841.

[6] A. Pereira, J.L. Akasaki, J.L.P. Melges, M.M. Tashima, L. Soriano, M.V. Borrachero, J. Monzó, J. Payá, Mechanical and durability properties of alkali-activated mortar based on sugarcane bagasse ash and blast furnace slag, Ceram. Int. 41 (2015) 13012-13024.

[7] V.N. Castaldelli, J.L. Akasaki, J.L.P. Melges, M.M. Tashima, L. Soriano, M.V. Borrachero, J. Monzó, J. Payá, Use of Slag/Sugar Cane Bagasse Ash (SCBA) blends in the production of alkali-activated materials, Materials 6 (2013) 3108-3127.

[8] J.C.B. Moraes, J.L.P. Melges, J.L. Akasaki, M.M. Tashima, L. Soriano, J. Monzó, M.V. Borrachero, J. Payá, Pozzolanic Reactivity studies on a biomass-derived waste from sugar cane production: Sugar Cane Straw Ash (SCSA), ACS Sust. Chem. Eng. 4 (2016) 4273-4279.

[9] Sugarcane production, UNICA – União da Indústria de Cana-de-Açúcar Website, http://www.unicadata.com.br/index.php?idioma=2

[10] B.S. Moraes, M. Zaiat, A. Bonomi, Anaerobic digestion of vinasse from sugarcane ethanol production

558 in Brazil: Challenges and perspectives, Renew. Sust. Energ. Rev. 44 (2015) 888-903.
559 [11] M.R.L.V. Leal, M.V. Galdos, F.V. Scarpare, J.E.A. Seabra, A. Walter, C.O.F. Oliveira, Sugarcane straw
560 availability, quality, recovery and energy use: A literature review, Biomass Bioenerg. 53 (2013) 11-19.
561 [12] J.M. Mesa-Pérez, J.D. Rocha, A. Barbosa-Cortez, M. Penedo-Medina, C.A. Luengo, E. Cascarosa, Fast
562 oxidative pyrolysis of sugar cane straw in a fluidised bed reactor, Appl. Therm. Eng. 56 (2013) 167-175.
563 [13] S.V. Lemos, M.S. Denadai, S.P.S. Guerra, M.S.T. Esperancini, O.C. Bueno, I.C. Takitane, Economic efficiency
564 of two baling systems for sugarcane straw, Ind. Crop. Prod. 55 (2014) 97-101.
565 [14] C. Shi, P.V. Krivenko, D. Roy, Alkali-Activated Cements and Concretes, Taylor & Francis, London and New
566 York, 2006.
567 [15] M.M. Tashima, J.L. Akasaki, J.L.P. Melges, L. Soriano, J. Monzó, J. Payá, M.V. Borrachero, Alkali activated
568 materials based on fluid catalytic cracking catalyst residue (FCC): Influence of SiO_2/Na_2O and H_2O/FCC ratio on
569 mechanical strength and microstructure, Fuel 108 (2013) 833-839.
570 [16] I. Ozer, S. Soyer-Uzun, Relations between the structural characteristics and compressive strength in metakaolin
571 based geopolymers with different molar Si/Al ratios, Ceram. Int. 41 (2015) 10192-10198.
572 [17] S. Aydin, B. Baradan, Effect of activator type and content on properties of alkali-activated slag mortars,
573 Compos. Part B 57 (2014) 166-172.
574 [18] S.A. Bernal, R.S. Nicolas, J.S.J. van Deventer, J.L. Provis, Alkali-activated slag cements produced with a
575 blended sodium carbonate/sodium silicate activator, Adv. Cem. Res. 28 (2016) 262-273.
576 [19] N. Bouzón, J. Payá, M.V. Borrachero, L. Soriano, M.M. Tashima, J. Monzó, Refluxed rice husk ash/NaOH
577 suspension for preparing alkali activated binders, Mater. Lett. 115 (2014) 72-74.
578 [20] F. Puertas, M. Torres-Carrasco, Use of glass waste as an activator in the preparation of alkali-activated slag.
579 Mechanical strength and paste characterisation, Cem. Concr. Res. 57 (2014) 95-104.
580 [21] H.K. Tchakouté, C.H. Rüscher, S. Kong, E. Kamseu, C. Leonelli, Comparison of metakaolin-based geopolymer
581 cements from commercial sodium waterglass and sodium waterglass from rice husk ash, J. Sol-Gel. Sci. Technol. 78
582 (2016) 492-506.
583 [22] S. Song, H.M. Jennigs, Pore solution chemistry of alkali-activated ground granulated blast-furnace slag, Cem.
584 Concr. Res. 29 (1999) 159-170.

585 [23] J.I. Escalante-Garcia, A.F. Fuentes, A. Gorokhovsky, P.E. Fraire-Luna, G. Mendonza-Suarez, Hydration
586 products and reactivity of blast-furnace slag activated by various alkalis, J. Am. Ceram. Soc. 86 (2003) 2148-53.
587 [24] I. Ismail, S.A. Bernal, J.L. Provis, R.S. Nicolas, S. Hamdan, J.S.J. van Deventer, Modification of phase
588 evolution in alkali-activated blast furnace slag by the incorporation of fly ash, Cem. Concr. Compos. 45 (2014) 125-
589 135.
590 [25] M.A. Salih, N. Farzadnia, A.A.A. Ali, R. Demirboga, Development of high strength alkali activated binder
591 using palm oil fuel ash and GGBS at ambient temperature, Constr. Build. Mater. 93 (2015) 289-300.
592 [26] D. Ravikumar, N. Neithalath, Effects of activator characteristics on the reaction product formation in slag
593 binders activated using alkali silicate powder and NaOH, Cem. Concr. Compos. 34 (2012) 809-818.
594 [27] A.F. Abdalqader, F. Jin, A.A. Al-Tabbaa, Development of greener alkali-activated cement: utilisation of
595 sodium carbonate for activating slag and fly ash mixtures, J. Clean. Prod. 113 (2016) 66-75.
596 [28] H. El-Didamony, A.A. Amer, H.A. Ela-ziz, Properties and durability of alkali-activated slag pastes immersed in
597 sea water, Ceram. Int. 38 (2012) 3773-3780.
598 [29] S. Mindness, J.F. Young, D. Darwin, Concrete, second ed., Pearson, London, 2002.
599 [30] D. Zaharaki, K. Komnitsas, Effect of additives on the compressive strength of slag-based inorganic polymers,
600 Global NEST Journal 11 (2009) 137-146.